



# PERLE : A High Power Energy Recovery Facility for Europe

## A Contribution to the Update of the European Strategy on Particle Physics

Cockcroft Institute, AsTEC Daresbury, TU Darmstadt, BINP Novosibirsk, CERN, Liverpool University,  
IPN and LAL Orsay, Thomas Jefferson Laboratory, CEA Saclay +

Contact Persons: Max Klein (Liverpool) and Achille Stocchi (Orsay)

### Executive Summary

The efficient recovery of power, to re-excite cavities from the used beam, was proposed in 1965. Major advances in superconducting RF technology, as quantified by cavity quality factors  $Q_0$  in excess of  $10^{10}$ , and the consideration of multi-turn recirculator passages, have opened the door to the *green* generation of high energy, high brightness, high current electron beams. The facility PERLE, here presented to the formation of the European Strategy for Particle Physics, is being designed as a new generation facility reaching for the first time into the 10 MW power regime of beam current and energy. The PERLE Collaboration comprises currently ten institutions. With Daresbury (UK), Darmstadt (D), Jlab (US) and Novosibirsk (Ru) there are four laboratories, which have been pioneering the development of ERL technology, together with three leading laboratories on SRF technology, CERN, Orsay (LAL and IPN) and Saclay CEA, and others. PERLE has been designed in support of the LHeC development, which defines its configuration (3 turn recirculator), its frequency (802 MHz, synergetic with FCC requirements) and electron current (20 mA or 500 pC in the LHC, 40 MHz time structure). This contribution, based on the 2017 PERLE CDR [1] and recent progress, describes the purpose, the parameters and configuration as well as the main components, including the successfully built first 802 MHz SC Niobium cavity with a large dynamic range and a  $Q_0$  exceeding  $3 \cdot 10^{10}$ . Based on in-kind contributions including re-use of existing components, especially the source (Daresbury, ALICE) and cryomodule (CERN, SPL), PERLE is expected to be operational at Orsay in the early twenties in an initial configuration subsequently upgradeable to full energy. The facility has the main goal of developing ERL technology, especially SRF, for application in high energy colliders, especially LHeC and FCC, as well as to develop techniques for multi-turn, high current ERL operation, complementary to and collaborating with the upcoming 1.3 GHz facilities CBETA at Cornell and bERLinPro and others. As such it represents a major contribution to the development of energy and intensity frontier accelerators, the innovation through technology of which compares well with plasma wakefield R&D for high gradient acceleration. The uniquely demanding parameters of PERLE make it a most powerful facility for lower energy precision electron beam physics in the areas of electroweak interactions, proton radius, search for dark bosons, or for the investigation of the unknown charge density of heavy nuclei such as the magic  $^{132}\text{Sn}$  as a striking example for a PERLE nuclear physics programme. From PERLE a 5 MeV energy photon beam can be derived of an intensity more than a factor of 100 higher than at ELI, which is a base for novel photo-nuclear physics or the production of medical radio-isotopes. As this paper is being submitted, the leading laboratories are signing Memoranda of Understanding for the foundation of the PERLE Collaboration. Being hosted at Orsay, in one of CERN's larger "satellite" laboratories, PERLE is ideally suited to support our joint particle physics future at CERN and to also maintain more than one of our larger associated research infrastructures at the highest level, for Europe and beyond.

# 41 1 Energy Recovery and the Mission of PERLE

42 PERLE will be a unique and leading edge facility designed to push advances in accelerator technology, to  
43 provide intense and highly flexible test beams for material and component development, and ultimately  
44 a foundation for unique particle and radiation sources for a wide array of applications. Energy recovered  
45 linacs (ERL's) are just beginning to assert their potential as game changers in the field of accelerators and  
46 their applications. Their unique combination of bright, linac-like beam quality with high average current  
47 and extremely flexible time structure, unprecedented operating efficiency and compact footprint opens the  
48 door to previously unattainable performance regimes.

49 LHeC offers the promise of an exciting and realisable near term addition to the capability of LHC, opening  
50 up a whole new world of electron-hadron physics at unprecedented energy and luminosity, made possible  
51 only by ERL technology. While the concept and promise of ERL's has been kick-started by demonstration  
52 machines based on existing accelerator technology, PERLE will be the first machine designed from the  
53 ground up to use fully optimised ERL-specific designs and hardware. PERLE will include and validate all  
54 the critical elements needed for LHeC on an affordable scale but with uncompromising beam parameters  
55 including average and peak beam current, emittance, three pass acceleration and energy recovery, optimised  
56 recirculation optics, and insertion regions for component, material and instrumentation testing. In the future  
57 these facilities can be used to develop novel insertion devices, damage resistant intercepting diagnostics and  
58 thin targets, high dynamic range and multi-pass beam position monitors, etc. PERLE will be the only ERL  
59 facility worldwide to incorporate all these features in the foreseeable future. The flexible bunch timing made  
60 possible by the advanced photo-injector will allow for beam testing of SRF structures with a wide range of  
61 frequencies at high intensities.

62 PERLE is of special importance for CERN: its RF group is committed to the operation, maintenance and  
63 upgrade of the RF systems of the LHC and its injector chain, as well as to the preparation of technologies  
64 and know-how required for future accelerators. Superconducting RF is clearly amongst the key technologies,  
65 and there is strong synergy of PERLE with the requirements of the LHC, its High-Luminosity upgrade and  
66 the different flavours of the FCC study. The PERLE frequency was chosen to be the exact harmonic of  
67 the LHC frequency (and equal to the SPS Landau system), such that the work for PERLE will directly  
68 profit from other SRF activities at CERN. Ultimately PERLE can be used as test facility for cavities and  
69 cryomodules for LHC and its injectors, and to validate LHeC and FCC concepts and hardware.

70 PERLE has synergy, especially with the upcoming 1.3 GHz facilities CBETA at Cornell, bERLinPro at  
71 Berlin and MESA at Mainz. A global Technical ERL Collaboration is being formed to address common  
72 issues and exchange expertise, which also includes BINP, CEBAF, Daresbury, KEK and the 3 GHz facility  
73 S-DALINAC at Darmstadt, currently the only ERL facility operational in Europe.

74 Once built, PERLE will be a magnet for researchers seeking to use the unique capabilities to test new  
75 ideas in beam and accelerator physics, develop new photon sources, perform exciting low energy particle  
76 and nuclear physics experiments and develop new materials and components for future applications. Subse-  
77 quently, the parameters, the lattice configuration, the site and main components are briefly presented in an  
78 introductory style. The contribution ends with a sketch on milestones and cost, followed by an Appendix  
79 on the exciting particle and nuclear physics potential of PERLE.

## 80 2 Parameters

81 The main parameters of the here presented ERL facility are summarised in Tab. 1. Subsequently the choice  
82 of frequency and luminosity issues are discussed which are inherent to these basic characteristics of PERLE.

### 83 2.1 Choice of Frequency

84 In order to assure continuous electron-proton collisions, the RF buckets of the electron ERL must match to  
85 the bunch positions of the proton bunches in the LHC. A key requirement for this to happen is that the RF  
86 system of the ERL has a harmonic number that matches the proton bunch spacing in the LHC. Initial studies  
87 for the LHeC and PERLE RF system had investigated the options of using either the 1.3 GHz ILC type or the

Parameter	Target Value
Injection energy [MeV]	7
Maximum energy [MeV]	500
Normalised emittance $\gamma\varepsilon_{x,y}$ [mm mrad]	6
Electron beam current [mA]	20
Bunch spacing [ns]	25
Bunch length (rms) [mm]	3
RF frequency [MHz]	801.58
Duty factor	CW

Table 1: Basic Parameters of PERLE at Orsay

704.42 MHz ESS and SPL type cavities in order to profit from existing recent SRF developments. However, the LHC utilises a 400.8 MHz main RF system and features a bunch spacing of 40.079 MHz. Unfortunately neither the ILC nor the ESS and SPL cavities have a harmonic frequency to the LHC bunch spacing. Both cavity types are approximately 20 MHz away from a harmonic of the LHC bunch spacing. Both cavity types would therefore have to be modified [frequency change] for use in LHeC.

It was therefore decided to engage in a selection of the optimum ERL SRF frequency based on basic requirements for the ERL operation: the overall beam stability - or the ability to operate at high beam currents - and the power requirements for operating the ERL. Studies on the transverse beam stability in the SRF system in the presence of Higher Order Modes have shown that lower RF frequencies, below 1 GHz, provide a better damping of transverse excitations and should therefore be better suited for reaching the goal of high current operation in the ERL [2]. Studies on the overall power requirements point towards an SRF frequency choice in the range of 700 MHz and 1050 MHz for small grain Nb and 300 MHz and 800 MHz for large grain Nb cavities [3]. Combining the two options of small and large grain Nb cavities one obtains an optimum RF frequency window of 700 MHz to 800 MHz.

The next decision driver for the SRF frequency choice for the ERL is to look for synergies with other future accelerator projects. The FCC is studying 802 MHz RF systems both for the FCC-ee as well as for the FCC-hh projects. This frequency is exactly twice that of the nominal HL-LHC RF system. Therefore this frequency was adopted for the ERL, both in the LHeC and PERLE, and engaged in an SRF R&D program with JLab in synergy with the FCC study.

## 2.2 Current and Luminosity

The luminosity of the LHeC is determined by the brightness of the proton beam, its beta function and the electron current. It has been shown in [4] that a peak luminosity as high as  $L \simeq 10^{34} \text{ cm}^{-2}\text{s}^{-1}$  can be obtained with an electron current of order 20 mA. The provision of such a current, the resulting six-fold load of the cavities, in excess of 100 mA as well as the verification of a high  $\eta$  in multi-turn operation are characteristic demands for why PERLE has to be built.

The luminosity of  $ep$  scattering with PERLE itself is given as  $L = \rho l N_A N_e$ . For a hydrogen target of density  $\rho = 0.07 \text{ g cm}^{-3}$  and length  $l = 10 \text{ cm}$  one gets  $L = 4.3 \cdot 10^{23} \text{ cm}^{-2} N_e$ . For a source delivering 500 pC of charge and a 25 ns bunch spacing one obtains a current corresponding to about  $1.2 \cdot 10^{17} \text{ e s}^{-1}$ . As a consequence the luminosity for elastic  $ep$  scattering can be expected to be as high as  $4 \cdot 10^{40} \text{ cm}^{-2}\text{s}^{-1}$ , with a 10 cm proton target at 20 mA current.

## 2.3 Photon Beam Characteristics

A gamma-ray beam of maximum energy of 4.5 MeV (9.1 MeV) can be produced from the Compton Scattering of a laser beam of 1030 nm (515 nm) wavelength onto the PERLE electron bunches. LAL demonstrated routinely power stacking of 200 kW in a resonant cavity. For a laser beam mode matched with the electron bunch sizes the expected gamma-ray flux is  $7.0 \cdot 10^{10} \gamma/\text{s}$  for a laser beam wavelength of 1030 nm and

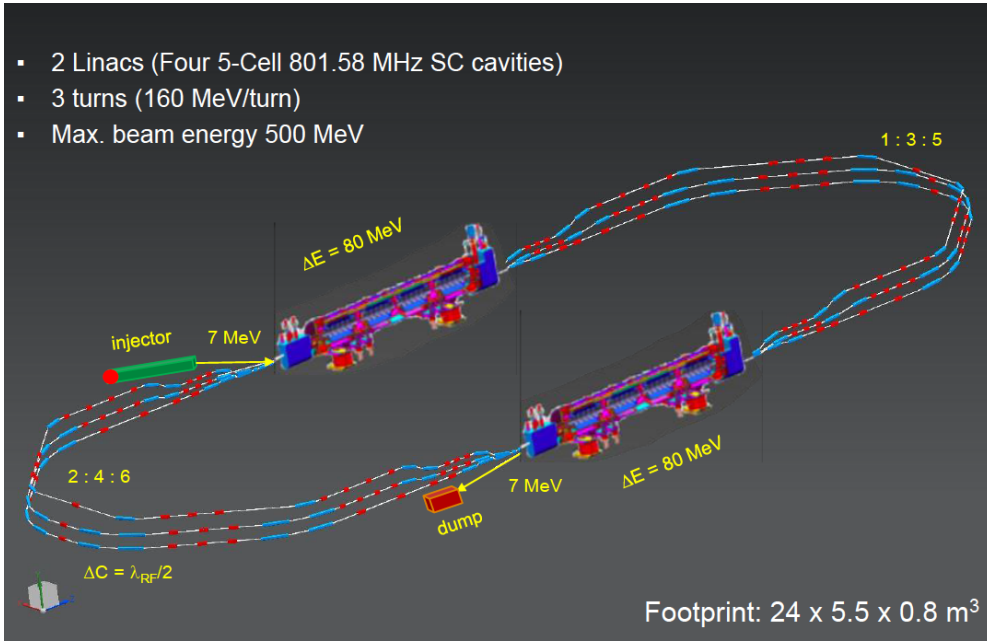


Figure 1: PERLE layout featuring two parallel linacs each hosting a cryomodule housing four 5-cell SC cavities, achieving 500 MeV in three passes.

123  $3.5 \cdot 10^{10} \gamma/s$  for 515 nm. A small crossing angle is required (below  $5^\circ$ ) that is achievable in an arc section of  
 124 PERLE. The intensity is by at least two orders of magnitude higher than that at the ELI facility [5].

### 125 3 Configuration and Lattice

126 The PERLE accelerator complex is arranged in a racetrack configuration hosting two cryomodules (con-  
 127 taining four, 5-cell cavities operating at 802 MHz), each located in one of two parallel straights completed  
 128 with a vertical stack of three recirculating arcs on each side. The straights are 10 m long and the  $180^\circ$  arcs  
 129 are 5.5 across. Additional space is taken by 4 m long spreaders/recombiners, including matching sections.  
 130 As illustrated in Fig. 1, the total footprint of PERLE is:  $24 \times 5.5 \times 0.8 \text{ m}^3$ , accounting for 40 cm vertical  
 131 separation between arcs. Each of the two cryomodules provides up to 82 MeV energy boost. Therefore, in  
 132 three turns, a 492 MeV energy increase is achieved. Adding the initial injection energy of 7 MeV yields the  
 133 total energy of approximately 500 MeV.

134 Multi-pass energy recovery in a racetrack topology with identical linacs explicitly requires that both the  
 135 accelerating and decelerating beams share the individual return arcs. Therefore the TWISS functions at  
 136 the linac ends have to be identical, for both the accelerating and decelerating linac passes converging to the  
 137 same energy and therefore entering the same arc. Injection at 7 MeV into the first linac is done through a  
 138 fixed field injection chicane, with its last magnet (closing the chicane) being placed at the beginning of the  
 139 linac. It closes the orbit bump at the lowest energy, injection pass, but the magnet (physically located in  
 140 the linac) will deflect the beam on all subsequent linac passes. In order to close the resulting higher pass  
 141 bumps, the so-called reinjection chicane is instrumented, by placing two additional bends in front of the last  
 142 chicane magnet. This way, the re-injection chicane magnets are only visible by the higher pass beams. The  
 143 spreaders are placed directly after each linac to separate beams of different energies and to route them to  
 144 the corresponding arcs. The recombiners facilitate just the opposite: merging the beams of different energies  
 145 into the same trajectory before entering the next linac.

146 The spreader design consists of a vertical bending magnet, common for all three beams, that initiates  
 147 the separation. The highest energy, at the bottom, is brought back to the horizontal plane with a chicane.  
 148 The lower energies are captured with a two-step vertical bending. The vertical dispersion introduced by

149 the first step bends is suppressed by the three quadrupoles located appropriately between the two steps.  
150 The lowest energy spreader is configured with three curved bends following the common magnet, because  
151 of a large bending angle ( $45^\circ$ ) the spreader is configured with. This minimizes adverse effects of strong  
152 edge focusing on dispersion suppression in the spreader. Following the spreader there are four matching  
153 quads to bridge the TWISS function between the spreader and the following  $180^\circ$  arc (two betas and two  
154 alphas). All six,  $180^\circ$  horizontal arcs are configured with Flexible Momentum Compaction (FMC) optics to  
155 ease individual adjustment of M56 in each arc (needed for the longitudinal phase-space reshaping, essential  
156 for operation with energy recovery) . The lower energy arcs (1, 2, 3) are composed of four 45.6 cm long  
157 curved  $45^\circ$  bends and of a series of quadrupoles (two triplets and one singlet), while the higher arcs (4, 5,  
158 6) use double length, 91.2 cm long, curved bends. The usage of curved bends is dictated by a large bending  
159 angle ( $45^\circ$ ). If rectangular bends were used, their edge focusing would have caused significant imbalance of  
160 focusing, which in turn, would have had adverse effect on the overall arc optics. Another reason for using  
161 curved bends is to eliminate the problem of magnet sagitta, which would be especially significant for longer,  
162 91.2 cm, bends. Each arc is followed by a matching section and a recombiner (both mirror symmetric to  
163 previously described spreader and matching segments). As required in case of identical linacs, the resulting  
164 arc features a mirror symmetric optics (identical betas and sign reversed alphas at the arc ends). Complete  
165 lattice calculations can be found in [1].

166 The presented arc optics with modular functionality facilitates momentum compaction management  
167 (isochronicity), as well as orthogonal tunability for both beta functions and dispersion. The path-length of  
168 each arc is chosen to be an integer number of RF wavelengths except for the highest energy pass, arc 6,  
169 whose length is longer by half of the RF wavelength (to shift the RF phase from accelerating to decelerating,  
170 switching to the energy recovery mode).

## 171 4 Orsay: The Site

172 LAL and IPN Orsay intend to host the 500 MeV PERLE version. The footprint of this facility occupies  
173 a rectangle of  $24 \times 5.5 \text{ m}^2$ . This area should be enclosed by shielding at a sufficient distance to allow  
174 passage and maintenance operations. We estimate the required passage and half thickness of the accelerator  
175 component to 2 m. A concrete shielding is assumed here to stop photons and neutrons produced by halo  
176 electrons. Detailed study of the radiation generated by the impinging electron will be necessary at a later  
177 stage. An increase of the shielding required could be alleviated by the use of denser materials. In addition,  
178 the PERLE operation at the design beam parameters (Tab.1) require an in depth study of the machine  
179 failure scenario to measure and control the beam losses in order to estimate the radiation dose outside the  
180 accelerator room, besides the CDR design of the beam dump [1]. This study is currently ongoing and the  
181 outcomes of it will have an impact on the site and the safety provisions to be implemented. Besides the  
182 central area required for machine implementation, space needs to be allocated for the auxiliary systems  
183 (power converters for magnets, septa and kickers, RF power, Water cooling, Cryogenics, Electron source,  
184 Dump). One has also to consider sufficient area for experiments that may use the PERLE beam. As a rough  
185 estimate one would need to triple the area of the accelerator itself to accommodate all services shielding  
186 included. The building that would host this version of PERLE is a former experimental hall, Super ACO  
187 hall. It is equipped with cranes and electricity. The ground of the building is made of concrete slabs with  
188 variable ground resistance. More than half of the hall area has a sufficient resistance to allow the installation  
189 PERLE. Being next to the tunnel of the old Orsay linac and close to the "Igloo", where new accelerators  
190 are being installed currently, the building is partially shielded and some equipment (water-cooling circuits,  
191 electrical transformer) can be shared with the other machines. The building gives the possibility to install  
192 the RF source and the power supplies at a different level than the accelerator. An existing control room  
193 that overlooks the experimental hall could be used for PERLE. Since all the accelerators installed nearby  
194 are based on warm technology, a cryogenic plant will be built. All the needed support for infrastructure is  
195 fully assured. Altogether, this appears to be a well suitable place which has the advantage to be available.

## 196 5 Components

### 197 5.1 Source and Injector

198 The PERLE injector must be capable of delivering a 20 mA beam comprising of 500 pC bunches with a  
199 repetition rate of 40.1 MHz. To provide efficient injection and acceleration of the beam in the ERL, its  
200 emittance should be less than  $6\text{ mm mrad}$  with a bunch length of 3 mm at the injection energy of 7 MeV.  
201 There is also the possibility of delivering polarised beams. To provide both these options a DC gun based  
202 injector will be used. The beam will be provided with a photocathode illuminated by laser pulses with the  
203 required time structure. The acceleration of the beam in the injection beam line to the necessary energy  
204 will be done with a booster operating with a frequency of 801.58 MHz, the same frequency as the main ERL  
205 linacs. The booster linac, under design, will consist of five cavities with independently controllable phases  
206 and amplitudes. The longitudinal bunch compression will be done using a (sub) harmonic RF buncher and  
207 the booster. Independent control of the booster cavities allows for fine adjustment of the bunching and  
208 acceleration. Focusing solenoids will be used for transport of the beam and for emittance compensation  
209 which reduces the emittance growth due to the significant space charge forces present. After the booster the  
210 beam is transported to the main ERL loop and injected with a merger. In order to linearise the longitudinal  
211 phase space the installation of an additional linearisation cavity is being considered. The polarised operation  
212 mode will require the addition of a spin rotator section between the gun and the booster.

213 The PERLE photocathode gun will initially be the DC gun previously used on the ALICE ERL based  
214 at Daresbury. The required upgrade for operation with high average current will be based on one previously  
215 designed for ALICE. First of all, a load lock system allowing photocathode replacement without breaking  
216 the vacuum will be installed. The significantly higher bunch charge of PERLE compared to ALICE requires  
217 a re-optimisation of the gun electrode system. For unpolarised and polarised operation modes of PERLE  
218 the gun will run at different operating voltages. The operating voltage for the unpolarised mode will be  
219 350 kV while for the polarised mode it will be lower, 220 kV, to provide longer photocathode lifetime and  
220 more effective spin manipulation. The upgrade will add a movable anode which should allow its distance to  
221 the cathode to be varied and to set the optimal value for the desired operating voltage.

222 Antimonide based photocathodes will be used for the unpolarised operation mode of PERLE. These  
223 materials have high quantum efficiency in the wavelength range where lasers with sufficient power to provide  
224 required average current are available. The polarised operation mode of the PERLE injector requires to use  
225 gallium arsenide based photocathodes as the only materials capable of delivering a polarised beam.

### 226 5.2 Cavity Prototype and Design

227 Activities to optimize a bare 802 MHz five-cell ERL linac cavity design, to build a prototype and to validate  
228 the design in a vertical test at 2 K helium temperature have been successfully completed at Jlab in 2018.  
229 The chosen *high current* cell contour shape aimed to balance key performance parameters with regard  
230 to RF, mechanical and beam-dynamical aspects, e.g. resulting in a rather large cell-to-cell coupling that  
231 considers efficient Higher-Order-Mode (HOM) damping, while keeping the magnetic and electric surface RF  
232 peak fields as well as the dynamic heat load at a given accelerating field comparably small [6]. A full set of  
233 parameters for this cavity can be found in the PERLE CDR [1], version called Jlab2 in Table 4.4.

234 An adequate HOM coupler technology for the cavity is being developed. A possible, comparably compact  
235 concept is considered with a single HOM endgroup located outside the helium vessel but close to the cavity.  
236 It accommodates three coaxial, actively cooled (LHC-style) HOM couplers. The usage of three coaxial  
237 couplers ( $120^\circ$  apart in azimuth) will allow capturing different transverse mode polarizations efficiently.

238 Though the prototype efforts focused on the five-cell cavity development, JLab also produced single-cell  
239 cavities, i.e. one further Nb cavity and two OFHC copper cavities. The former has been shipped to FNAL  
240 for N-doping/infusion studies, whereas the latter were delivered to CERN for ongoing Nb thin-film coating  
241 R+D. In addition, a copper cavity was built for low power bench measurements, for which multiple half-cells  
242 can be mechanically clamped together. Presently, a mock-up can be created with up to two full cells. This  
243 cavity has been produced in support of the HOM coupler development.

244 Initial results for the Nb cavities - made from fine grain high-RRR Nb - were encouraging since both

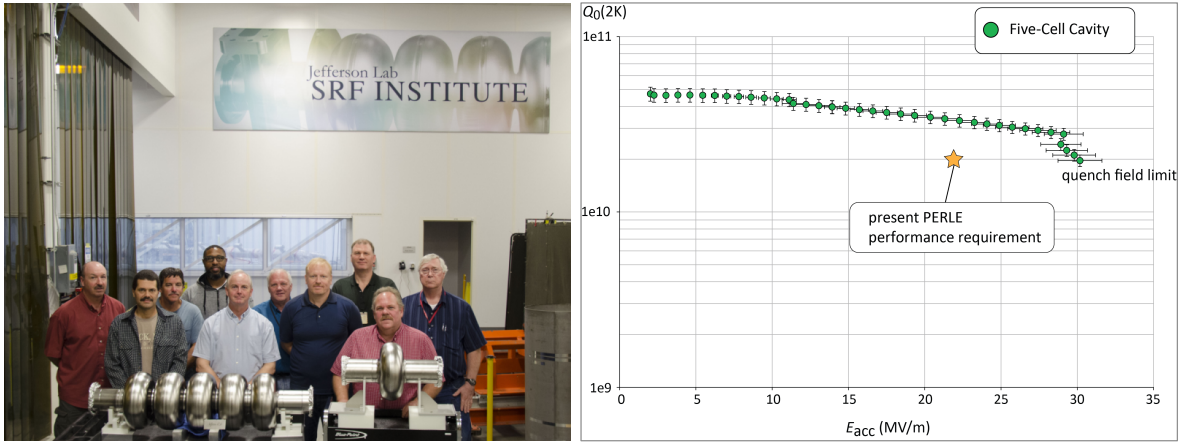


Figure 2: Left: Jlab team behind the 5-cell and a single cell Niobium cavity; Right: Vertical test result of the five-cell 802 MHz Niobium cavity. The yellow star indicates the edge of the performance considered for operation of PERLE with a typical CW gradient optimum around 20 MV/m.

245 cavities reached accelerating fields,  $E_{acc}$ , slightly above 30 MV/m ultimately limited by thermal breakdown  
 246 (quench). Moreover, the RF losses were rather small due to the relatively rather low RF frequency, which  
 247 provides a small BCS surface resistance. This resulted in unloaded quality factors,  $Q_0$ , well above  $4 \cdot 10^{10}$   
 248 at 2 K at low fields, while  $Q_0$ -values beyond  $3 \cdot 10^{10}$  could be maintained for the five-cell cavity up to about  
 249 27 MV/m (see Fig. 2). Only standard interior surface post-processing methods were applied, including bulk  
 250 buffered chemical polishing, high temperature vacuum annealing, light electropolishing, ultra-pure high-  
 251 pressure water rinsing, and a low temperature bake-out.

252 While the vertical test results indicate generous headroom for a potential performance reduction once a  
 253 cavity is equipped with all the ancillary components and installed in a cryomodule, clean cavity assembly  
 254 procedure protocols must be established for the cryomodules to minimise the chance of introducing field-  
 255 emitting particulates.

### 256 5.3 Cryomodule Design

257 The PERLE layout is integrating two superconducting RF cryomodules, one per linac, each of them contain-  
 258 ing 4 superconducting 801.58 MHz 5-cell elliptical cavities. In addition to the classic constraints of an SRF  
 259 cryomodule, several requirements are quite specific to the ERL operating mode posing several challenges.  
 260 The most important one is linked to the CW operation of the cryomodules, where dynamic heat loads are  
 261 much larger than static ones. Thus, reaching high quality factors (low cryogenic losses) for the SC cavities  
 262 is a main objective. Besides specific optimisation on cavity design and preparation, the cryomodule has  
 263 to provide a very low residual magnetic field environment to the cavity. To achieve that, both stringent  
 264 optimisation of the magnetic shielding (material, numbers of layers, active and/or passive shielding) and  
 265 careful choices of the non-magnetic material for components located close to the cavities are required. Even  
 266 the cooling-down process has to be carefully studied to allow proper rejection of residual magnetic field in  
 267 the superconducting material (the so-called magnetic hygiene). Another important constraint is linked to  
 268 the rather high power to be extracted by the HOM couplers. The cryomodule has to provide the capacity to  
 269 efficiently evacuate the HOM thermal load not to degrade the cryogenic performances of the cryomodule.

270 Among the recent cryomodule developments made for several projects, we have chosen for PERLE to use  
 271 the cryomodule layout developed by IPN Orsay and CERN for the Superconducting Proton Linac (SPL) [7],  
 272 for its capacity to fulfil the PERLE requirements in terms of dimensions, cryogenic performances and cavity  
 273 requirements. In this cryomodule, the cavity string is directly supported by the power coupler with dedicated  
 274 inter-cavity support features. Moreover, it integrates a full length demountable top lid, enabling the cavity  
 275 string assembly from the cryomodule top. These two specific features allow an easier assembly process of  
 276 the cavity string inside the module as compared to other cryomodule designs. The thermal shield is made



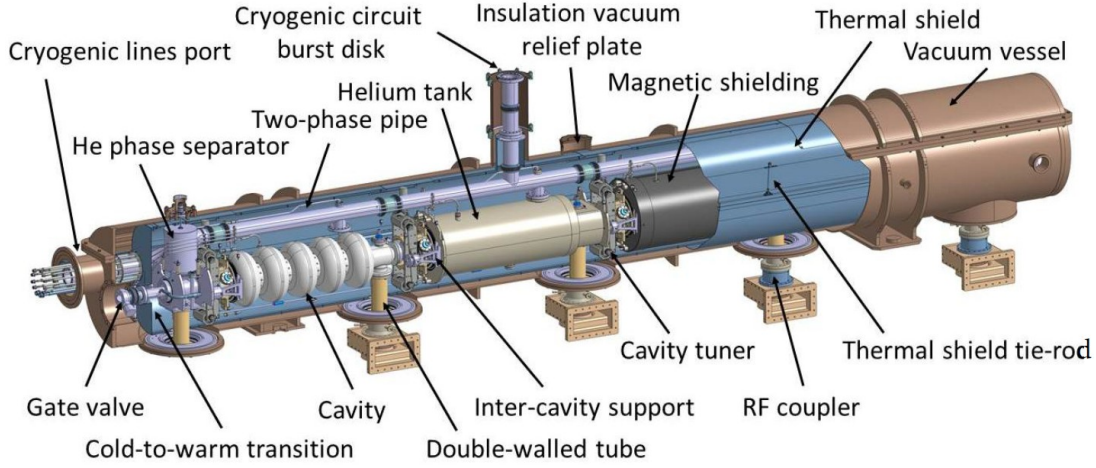


Figure 3: General assembly view of the SPL cryomodule considered to be adapted for PERLE.

277 of rolled aluminum sheets, and is composed of four main parts assembled before the vertical insertion of the  
 278 string of cavities. The shield, wrapped with multi-layer insulation, is suspended to the vacuum vessel  
 279 via adjustable tie rods in titanium alloy which also cope, by angular movements, with its thermal contractions.  
 280 The cavity stainless steel helium tanks are connected by a 100 mm-diameter two-phase pipe placed above  
 281 the cavities. This pipe ensures liquid feeding to the cavities by gravity, and is also used as a pumping line for  
 282 gaseous helium. The cavities are protected by individual magnetic shields made of 2 mm thick Cryoperm<sup>TM</sup>  
 283 sheets. The shields are made of 2 half-shells mounted around the helium tank and fixed to it on the tuner  
 284 side. This allows the residual magnetic field to be kept below about  $1 \mu\text{T}$ . The cryomodule provides a  
 285 dedicated 6 mm circuit supplies 4.5 K vapour helium for cooling of the RF coupler double-walled tubes.

286 The SPL R&D program already provided design and experimental results on this type of cryomodule,  
 287 and the mechanical capability of the module with the PERLE cavities has been checked requiring minor  
 288 adaptation of some internal parts. Even if additional studies have to be performed, once detailed designs of  
 289 some parts (like the HOM couplers) will be finalised, this cryomodule design is considered to be the reference  
 290 for the PERLE cryomodules.

## 291 5.4 Magnets

292 The inventory of the main magnets for PERLE lists 184 magnets, 24 dipoles and 114 quadrupoles in the  
 293  $2 \times 3$  arcs and 46 bending magnets in the two spreader/combiner sections. Their design optimisation is  
 294 ongoing. In the arcs, 24 bending magnets with vertical field are required (4 in each arc) with a  $45^\circ$   
 295 bending angle. They are distributed in two families with different magnetic length: 456 mm for arc 1 to 3 and  
 296 912 mm for arcs 4 to 6. The vertical aperture of the dipoles is 40 mm and a similar dimension is taken for  
 297 the horizontal good field region. The same cross-section is used for both families. In order to minimise the  
 298 distance between the arcs, an H type yoke, relatively narrow in vertical direction is foreseen. A feasibility  
 299 study has been done for both the short and the long model. A field homogeneity better than  $5 \cdot 10^{-4}$  is  
 300 obtained for each arc energy by optimising the width of the pole, the thickness of the shim and the pole  
 301 angle.

302 The 114 quadrupole magnets are distributed along the 6 arcs. In order to optimise the cost, they are  
 303 all the same with a magnetic length of 150 mm, an aperture diameter of 40 mm and an outer diameter of  
 304 250 mm. The highest gradient is 32.5 T/m and the harmonic content is lower than  $10^{-4}$  at 13 mm radius. In  
 305 the spreaders/combiners sections, 46 bending magnets with horizontal field and various deflection angles are  
 306 distributed in four families. Their magnetic lengths vary from 50 mm to 400 mm. The horizontal aperture  
 307 is 40 mm, and a similar dimension is taken for the vertical good field region.



## 308 6 Milestones, Cost and Time Schedule

309 The PERLE configuration, see Fig. 1, entails the possibility to construct PERLE in stages, starting by  
 310 installing a single linac in the first straight and initially replacing the second one by just beam lines. Such  
 311 a consideration is determined by the existence of the SPL cryomodule which will permit a rather rapid  
 312 realisation of a 250 MeV machine, in what currently and tentatively is considered Phase 1 of PERLE. This  
 313 will allow in relatively short term to test with beam, initially with the ALICE source, then upgraded to  
 314 higher currents (see Sect. 5.1) to examine various SRF components, to prove the multi-turn ERL operation  
 315 and to gain essential operation experience, described in detail in the PERLE CDR [1]. It is foreseen from  
 316 the beginning to size the infrastructure and equipment as for their final use (beam dump, cryogenics, cooling  
 317 circuit, shielding, electrical power, etc.). The cost of PERLE Phase 1 is estimated to be about 11 MEuro,  
 318 not including the cost of the Orsay infrastructure and the in-kind delivery of the source, the SPL cryomodule  
 319 and further components under discussion, which together represent another value of about 12 MEuro. The  
 320 second phase is for the realisation of PERLE at its design parameters, as a 10 MW machine with 500 MeV  
 321 energy from the production and installation of a dedicated further cryomodule, and the nominal current of  
 322 about 20 mA. Currents beyond 20 mA are of interest in a later stage of the PERLE operation. Upgrading  
 323 to PERLE Phase 2 requires an estimated extra 7 MEuro for the fully equipped cryomodule and possible  
 324 upgrade of equipment. A tentative time schedule for the realisation of PERLE at Orsay is presented in  
 Tab. 2.

Target Date	Milestone
May 2019	Dressed cavity design completion (HOM coupler, He tank)
Sept 2019	Adapted SPL cryomodule design completion
End 2019	Injection line (booster) design completion
Early 2020	Technical Design Report
Mid 2021	SPL cryomodule assembly
2022	Sequential installation at Orsay
2023	Phase 1 operation
2024	Second cryomodule completion
2025	Phase 2 operation

Table 2: Milestones, tentative, for PERLE at Orsay.

325

## 326 Appendix 1: Particle and Nuclear Physics with PERLE

327 The high energy, quality and intensity of the electron and photon beams obtained from PERLE make it  
 328 an outstanding low energy physics facility for numerous applications, some of which are sketched below.  
 329 This potential, or part of it, is supposed to be considered following the initial use of PERLE as a dedicated  
 330 accelerator R&D facility for establishing ERL as a reliable technology for the future of high energy and  
 331 nuclear physics.

### 332 Particle Physics

333 PERLE provides numerous opportunities beyond its primary aim as a testing ground for a future high-scale  
 334 ERL accelerator. Let us first mention a possible measurement of the electroweak mixing angle  $\sin^2 \theta_W$ ,  
 335 using elastic electron-proton scattering with a polarised beam. This possibility was recently explored for the  
 336 proposed P2 experiment at MESA. By detecting electrons at a scattering angle of about  $35^\circ$ , a polarisation  
 337 asymmetry of about  $10^{-7}$  can be measured in one year, corresponding to a precision of  $35 \times 10^{-5}$  in  $\sin^2 \theta_W$ .  
 338 This precision competes with the best high-energy measurement results, and provides a strong test of the  
 339 Standard Model in establishing the scale dependence. The weak mixing angle at low energies is also sensitive  
 340 to so-called *dark bosons*, a proposed solution to the dark matter puzzle involving light new particles akin  
 341 to the photon or the Z. These particles couple weakly to ordinary charged particles, and induce deviations

342 of  $\sin^2 \theta_W$  from its SM value at low  $Q^2$  [8]. The large beam energy and high beam intensity available at  
343 PERLE enhances the prospects for such measurements beyond that of existing proposals.

344 To fully exploit this potential, the uncertainties in the proton form factors need to be strongly reduced.  
345 This can be achieved in a first phase of experiments measuring the scattering distributions, at both forward  
346 and backward angles, with an unpolarised beam as has been discussed in the PERLE CDR [1]. These  
347 measurements can reduce the uncertainties in formfactors by an order or magnitude compared to present  
348 knowledge, and provide adequate precision for the measurement of  $\sin^2 \theta_W$ .

349 Finally, the discrepancy between the proton radius measured using electrons and muons constitutes  
350 another longstanding question. In elastic  $ep$  scattering, this quantity can be accessed through the slope of  
351 the electric form factor at  $Q^2 = 0$ . At PERLE, with a beam energy of 500 MeV or below, detecting scattered  
352 electrons down to  $4^\circ$  would allow to reach  $Q^2 \sim 10^{-4} \text{ GeV}^2$ , an order of magnitude below the limit of existing  
353 data. New data from PERLE would strongly reduce the uncertainty in the extrapolation to  $Q^2 = 0$ , and  
354 provide an excellent opportunity to consolidate the electron results.

## 355 Nuclear Physics

356 Our basic knowledge on the nuclear charge distributions was established on the stable nuclei using electron  
357 elastic scattering. Electrons of 400 – 800 MeV energy provide ideal spatial resolution scale of about 0.5 fm  
358 to study the interior nuclear charge distributions. As the electron-ion interaction mechanism is known to a  
359 high accuracy, direct expansion of the cross sections and the direct link to the charge distribution can be  
360 obtained, from which the proton distribution can be inferred.

361 The detailed proton density profiles are needed to add constraints on the proton correlations assumed  
362 within the nuclear models, and to explore the properties of the proton densities, in particular in the case  
363 of exotic nuclei having extended or exotic nuclear shapes (halo, clusters, bubbles) [9]. Up to now, due  
364 to the impossibility to perform ion-electron collisions with short-lived radioactive ions the knowledge on  
365 charge densities was limited to global relative radius changes provided by isotopic shifts observed in laser  
366 spectroscopy experiments.

367 From electron scattering data, however, much richer structure observables of the nuclear charge densities  
368 become accessible: i) global indication are the root mean square radii and diffuseness for the densities mod-  
369 elled as a simple analytical function, like the two parameter Fermi (2pF) function, as was done extensively  
370 for the stable nuclei reported in Nuclear data tables [10]; ii) In principle, if one can measure  $F(q)$  with an  
371 extended range of momentum transfer the interior proton density can be mapped via model independent  
372 analysis. The advent of PERLE would allow conceiving a program aiming at observing electron scattering  
373 from the interaction of the PERLE beam with a fixed self-confined target of 106 radioactive ions at relevant  
374 luminosities. A 2pF proton density distribution requires typical luminosities  $L$  of  $10^{24-28} \text{ cm}^{-2}\text{s}^{-1}$ , and for  
375 detailed densities (cross sections up to the second minimum, 3pF densities),  $L$  around  $10^{26-29} \text{ cm}^{-2}\text{s}^{-1}$ ,  
376 which are all easily achieved with PERLE. A typical achievable flagship case would be the determination,  
377 for the first time in nuclear-physics history, of the proton density of a doubly magic nucleus such as  $^{132}\text{Sn}$   
378 having an exceptionally large neutron-to-proton ratio.

## 379 Photo-Nuclear Physics

380 PERLE will also be operated as an intense source of quasi-monochromatic, energy-tunable, fully-polarised  $\gamma$   
381 radiation. The  $\gamma$ -ray beams will be produced by the process of Laser-Compton back-scattering on the intense  
382 relativistic electron beams of PERLE's third recirculation beam line providing  $\gamma$ -beam energies between 0.2  
383 and 5 MeV. PERLE's  $\gamma$ -ray beams can reach a significantly narrower bandwidth and simultaneously a much  
384 higher repetition rate than the Gamma Beam System at the Extreme Light Infrastructure - Nuclear Physics  
385 (ELI-NP), the new-generation facility currently under construction at Magurele, Romania.

386 Photonuclear reactions will significantly contribute to progress in the fields of nuclear structure physics,  
387 particle-physics metrology, nuclear astrophysics as it was exemplified in Ref. [1]. Apart from contributions  
388 to scientific research, photonuclear measurements at PERLE have a great potential for technological and  
389 commercial applications [11]. From the variety of research routes at PERLE's gamma-ray beam, we empha-  
390 sise the following three, only. i) The high-peak intensity gamma-ray beam at PERLE will make it possible

391 for the first time to directly measure the photoresponse of long-lived unstable nuclides, including a variety  
392 of actinides with halfives exceeding  $10^3$  years, such as  $^{230}\text{Th}$ ,  $^{231}\text{Pa}$ ,  $^{236,237}\text{Np}$ ,  $^{239,242,242}\text{Pu}$ ,  $^{247,248}\text{Cm}$  etc.  
393 because the beam's spectral density will produce a sufficiently significant signal even on light samples with  
394 a weight of the order of a milligram. This has not been technically feasible up to now. ii) Information on  
395 photonuclear reactions on unstable long-lived actinides is desired for a long time in the fields of nuclear  
396 structure, e.g., for quantifying the role of quadrupole-octupole collectivity in deformed actinides or assess-  
397 ing spin-flip partner orbitals in the Nilsson scheme of super-heavy nuclei, of nuclear astrophysics, e.g., for  
398 benchmarking photonuclear reaction rates in the fission-cycling of the rapid neutron-capture process in the  
399 nucleosynthesis in neutron-star mergers, or for applications in nuclear reactor technology, nuclear transmu-  
400 tation and nuclear safeguarding. iii) Moreover, photonuclear reactions are urgently needed in metrology for  
401 characterizing the low-spin excitation response of isotopes used for the detection of neutrinos or as detector  
402 materials in searches for beyond-standard model physics, such as  $0\nu\beta\beta$  decay or dark matter [1].

## 403 Acknowledgement

404  
405 The PERLE Collaboration acknowledges the important contributions of all authors of the CDR and at-  
406 tendees to workshops. It also is grateful for the emerging collaboration with the Technical ERL network  
407 of all facilities engaged globally in the development and applications of energy recovery. We are especially  
408 grateful for the initiative and guidance received by the CERN Directorate and by the International Advisory  
409 Committees for LHeC, chaired by Herwig Schopper, and for FCC, chaired by Guenter Dissertori.

410  
411 Work has been authored by Jefferson Science Associates, LLC under Contract No. DE-AC05-06OR23177  
412 with the U.S. Department of Energy.

## 413 References

- 414 [1] D. Angal-Kalinin et al. PERLE. Powerful energy recovery linac for experiments. Conceptual design report. *J. Phys.*,  
415 G45(6):065003, 2018.
- 416 [2] J. L. Abelleira Fernandez et al. A Large Hadron Electron Collider at CERN: Report on the Physics and Design Concepts  
417 for Machine and Detector. *J. Phys.*, G39:075001, 2012.
- 418 [3] Frank Marhauser. Frequency Choice for PERLE and Coupler Simulations. *Talk at PERLE Workshop, Orsay, 2017.*
- 419 [4] O. Bruening, J. Jowett, M. Klein, D. Pellegrini, D. Schulte, and F. Zimmermann. FCC-eh Baseline Parameters. *FCC-*  
420 *ACC-RPT-0012*, 2017.
- 421 [5] Fabian Zomer. Photon Beam Generation at PERLE. *Talk at LHeC Workshop, Orsay, 2015.*
- 422 [6] Frank Marhauser. Recent Results on a Multi-Cell 802 MHz bulk Nb Cavity. *Talk at FCC in Amsterdam, 2018.*
- 423 [7] V Parma et al. Status of the superconducting proton linac (SPL) cryomodule. *Proceedings of the 2013 Superconducting*  
424 *Radio Frequency Conference, Paris, 2013.*
- 425 [8] Hooman Davoudiasl, Hye-Sung Lee, and William J. Marciano. Muon g-2, rare kaon decays, and parity violation from dark  
426 bosons. *Phys. Rev.*, D89(9):095006, 2014.
- 427 [9] T. Duguet, V. Som, S. Lecluse, C. Barbieri, and P. Navrtil. Ab initio calculation of the potential bubble nucleus  $^{34}\text{Si}$ .  
428 *Phys. Rev.*, C95(3):034319, 2017.
- 429 [10] H. De Vries, C. W. De Jager, and C. De Vries. Nuclear charge and magnetization density distribution parameters from  
430 elastic electron scattering. *Atom. Data Nucl. Data Tabl.*, 36:495–536, 1987.
- 431 [11] G. Suliman et al. Gamma-beam industrial applications at ELI-NP. *Rom. Rep. Phys.*, 68 Suppl. II:799 – 846, 2016.